# Effect of Methionine Oxidation on the Structural Properties, Conformational Stability, and Aggregation of Immunoglobulin Light Chain LEN[†]

Dongmei Hu,[‡] Zhijie Qin,[‡] Bin Xue,[§] Anthony L. Fink,[‡,||] and Vladimir N. Uversky*[,§,⊥]

*Department of Chemistry, University of California, Santa Cruz, California 95064, Center for Computational Biology and Bioinformatics, Department of Biochemistry and Molecular Biology, Institute for Intrinsically Disordered Protein Research, Indiana University School of Medicine, Indianapolis, Indiana 46202, and Institute for Biological Instrumentation, Russian Academy of Sciences, 142290 Pushchino, Moscow Region, Russia*

*Received May 4, 2008; Revised Manuscript Received June 23, 2008*

ABSTRACT: Light chain amyloidoses arise from the overproduction and abnormal deposition of the immunoglobulin light chain in various organs. LEN is the variable domain of an immunoglobulin light chain originally isolated from the urine of a patient suffering from multiple myeloma, with no sign of renal dysfunction or amyloidosis. LEN was shown to form fibrils in vitro under mildly destabilizing conditions. In this work, we investigated the changes induced by methionine oxidation in the structural properties, conformational stability, and aggregation behavior of immunoglobulin light chain domain LEN. We established that LEN was well-protected from oxidation in its native state, but successful oxidation was achieved in the presence of 4 M GuHCl. Oxidation induced noticeable structural changes in LEN and destabilized this protein. The methionine-oxidized LEN preferred to form amorphous aggregates instead of fibrils. The results indicated that the LEN oxidation may play an important role in amorphous deposition of the protein, but not in its fibrillation.

The amyloidoses are lethal diseases involving the extracellular deposition of amyloid fibrils and plaques (*1, 2*). All amyloidoses arise from the conversion of specific proteins from their soluble functional states into stable, highly ordered, filamentous protein aggregates, known as amyloid fibrils, and from the deposition of these aggregated materials in a variety of organs and tissues (*3, 4*). Although the amyloid fibrils from different diseases are structurally and morphologically similar to each other, the amyloidogenic polypeptides causing diseases are extremely diverse and, prior to fibrillation, may be rich in $\beta$-sheet, $\alpha$-helix, or $\beta$-helix or be intrinsically disordered (*5*). The aggregation and subsequent development of protein deposition diseases originate from conformational changes in corresponding amyloidogenic proteins. In vitro studies show that the fibrils are produced from partially folded intermediates following either partial destabilization of physiologically folded proteins, in the case of globular proteins (*3–13*), or partial folding, in the case of natively unfolded (or intrinsically disordered) proteins (*5, 14–16*). Presumably, such a partially unfolded conformation enables specific intermolecular interactions, including electrostatic attraction, hydrogen bonding, and hydrophobic contacts, which are necessary for oligomerization and fibrillation.

There are four common light chain-related deposition diseases [AL amyloidosis,[1] light chain deposition disease (LCDD), myeloma cast nephropathy, and acquired Fanconi's syndrome], all arising from pathological deposition of light chains of monoclonal antibodies (*17–20*). Light chain amyloidosis originates from the overproduction and abnormal accumulation of light chain protein aggregates in various organs, with the most common organs affected being the kidney, heart, liver, and autonomic or peripheral nerves (*21*). AL amyloidosis is a rare disease, as only 1200−3200 new cases are reported each year in the United States, which is usually associated with myeloma. Amyloid deposits in organs affected by AL amyloidosis can cause shortness of breath, fatigue, edema (swelling of ankles and legs), dizziness upon standing, a feeling of fullness in the stomach (especially after eating), diarrhea, weight loss, enlarged tongue, numbness of the legs and arms, and protein in the urine.

As opposed to AL amyloidoses, LCDD is characterized by the deposition of amorphous, noncongophilic light chains in multiple organs. These deposits do not exhibit a fibrillar structure when examined ultrastructurally. As such, the morphology of the deposited light chain aggregates in AL amyloidoses and LCDD is clearly different. Patients typically exhibit only one form of light chain deposition. However,

[†] This research was supported in part by Grants R01 NS39985 (to D.H., Z.Q., and A.L.F.), R01 LM007688-01A1 (V.N.U.), and GM071714-01A2 (V.N.U.) from the National Institutes of Health. We gratefully acknowledge the support of the IUPUI Signature Centers Initiative.

* To whom correspondence should be addressed: Center for Computational Biology and Bioinformatics, Department of Biochemistry and Molecular Biology, Indiana University School of Medicine, 410 W. 10th St., HS 5009, Indianapolis, IN 46202. Phone: (317) 278-9650. Fax: (317) 278-9217. E-mail: vuversky@iupui.edu.

[‡] University of California.

[§] Indiana University School of Medicine.

[||] Died March 2, 2008.

[⊥] Russian Academy of Sciences.

[1] Abbreviations: AL amyloidosis, immunoglobulin light chain amyloidosis; LCDD, light chain deposition disease; ROS, reactive oxygen species; MSR, methionine sulfoxide reductase; MetO, methionine-oxidized; GuHCl, guanidinium hydrochloride; ThT, thioflavin T; CD, circular dichroism; ATR-FTIR, attenuated total reflectance Fourier transform infrared spectroscopy; EM, electron microscopy.

10.1021/bi800806d CCC: $40.75 
Published on Web 07/25/2008

there is at least one report of a patient exhibiting both AL amyloidosis and LCDD involving the same light chain (*22*).

Myeloma kidney or myeloma cast nephropathy occurs in the presence of excess free light chains in the plasma and urine. Although the mechanism by which urinary light chains lead to renal failure is not understood completely, it is believed that the pathology of this disease is associated with the precipitation of light chains in the tubules, leading to obstructing, dense, intratubular casts in the distal and collecting tubules that may initiate a giant cell reaction (*23*). Finally, acquired Fanconi's syndrome represents a complex of defects in the functioning of renal tubules associated with multiple myeloma.

Human antibody light chains originate from 30−40 $\kappa$ and $\lambda$ variable domain gene segments, each of which serves as the progenitor of a family of related light chains. Remarkable diversity of light chains is determined by the accumulation of somatic mutations. Therefore, the primary structures of amyloidogenic and nonamyloidogenic light chains differ at numerous sites, with no single amino acid substitution or combination thereof that would be responsible for the doubtless determination of a pathological propensity (*24*). Most variable domains form dimers at moderately high concentrations (a few milligrams per milliliter), and the dimerization constants and the geometry of the interface depend on the specific residues at the interface (*25*).

LEN is a 114-residue variable domain of the immunoglobulin light chain (*k*IV Bence Jones protein). Earlier, on the basis of the analysis of the amino acid sequences, LCs were classified in several groups and several hypervariable or complementarity-determining regions (CDRs) and framework regions were defined according to the sequence variability (*26*). According to the nomenclature of Kabat et al. (*26*), extra residues in CDR1, after residue 27, are labeled 27a−27f. There are six such extra residues in LEN (SVLYSS) and in other Bence Jones proteins from the *k*IV subgroup. Therefore, the numbering of their sequences traditionally goes from 1 (D) to 27 (Q), then from 27a to 27f, and then from 28 (S) to 108 (R). The crystal structure of LEN determined at 1.95 Å resolution revealed that this domain is a prototypical $\beta$-domain that consists of two $\beta$-sheets organized in a specific $\beta$-sandwich fold (*27*). The LEN X-ray crystal structure further indicated that hypervariable or complementarity-determining region 1 (CDR1) formed a large loop that extends out from the domain (*27*).

LEN was originally isolated from the urine of a patient suffering from multiple myeloma, with no sign of renal dysfunction or amyloidoses (*28*). However, LEN was shown to form fibrils in vitro under mildly destabilizing conditions (low pH or a certain amount of denaturant such as urea or GuHCl) (*29–31*). Benign LEN is very similar to amyloidogenic light chain domains, SMA and REC, which were initially extracted from the patients with AL amyloidosis (*28*). In fact, amino acid sequences of SMA and LEN are different at only eight positions, whereas REC is different from LEN at 14 positions (*28*). Interestingly, amyloidogenic LCs were shown to be significantly less stable than LEN in vitro (*24*). Furthermore, a series REC- or SMA-mimic mutations of LEN affected both the conformational stability and aggregation propensity of this protein (*24*). The systematic analysis of LEN structural properties and aggregation revealed the accumulation of two partially folded intermediates: a relatively nativelike intermediate that accumulated at pH values between 4 and 6 and a relatively unfolded, but compact, intermediate formed at pH <3. The unfolded intermediate was shown to readily form amyloid fibrils, whereas the nativelike intermediate preferentially assembled into the amorphous aggregates (*32*).

Protein oxidation is associated with numerous conditions characterized by oxidative stress, as well as a number of human diseases, including Alzheimer's disease, Parkinson's disease, diabetes, rheumatoid arthritis, muscular dystrophy, cataractogenesis, induction of renal tumors, bronchopulmonary dysplasia, amyloidosis, chronic ethanol ingestion, acute carbon tetrachloride toxicity, amyotrophic lateral sclerosis, and the progeria (*33*). All amino acid residues are potential targets for oxidation, which can be induced, for example, by $HO^{\bullet}$ generated upon exposure to ionizing radiation or in the presence of high concentrations of hydrogen peroxide and $Cu^{2+}$ or $Fe^{2+}$. Cysteine and methionine are by far the most sensitive to oxidation by almost all kinds of reactive oxygen species (ROS) (*34*). Methionine is easily oxidized to methionine sulfoxide by two-electron oxidation induced by $H_2O_2$, among many other biological oxidants (*35*). The methionine oxidation to methionine sulfoxide can be reversed by the methionine sulfoxide reductase (MSR) (*36, 37*). On the basis of this consideration, Levine et al. (*37*) proposed that the methionine oxidation in proteins might serve as a first line of antioxidant defense against ROS damage. In this work, we investigated the conformational changes of light chain domain LEN induced by methionine oxidation and analyzed the effect of oxidation on the conformational stability and aggregation of this protein. We found that the LEN was well-protected against oxidation in its native state. The methionine-oxidized (MetO) protein preferred to form amorphous aggregates instead of fibrils. The results indicate that oxidation of LEN could not play a role in its fibrillation.

## MATERIALS AND METHODS

*Chemicals.* Guanidine hydrochloride (GuHCl) with a purity of 99.5% was purchased from EM Science. Peptone and yeast extract used in the medium were purchased from Difco. All other chemicals were purchased from Fisher or Sigma and were of the highest available grade. The water was doubly deionized.

*Predictions of Intrinsic Disorder.* Disorder predictions for LEN were made using PONDR VSL2B (*38*) and FoldIndex (*39*) algorithms. PONDR VSL2 (version 2 Predictor Of Natural Disordered Regions, Various Short-Length) is an ensemble of logistic regression models that predicts per-residue order−disorder (*38*). Two models predict either long or short disordered regions, more than or fewer than 30 residues, based on features similar to those used by PONDR VLXT (*40*). The algorithm calculates a weighted average of these predictions, where the weights are determined by a meta predictor that approximates the likelihood of a long disordered region within its 61-residue window (*38*). FoldIndex, a freely available graphic web server (http://bioportal.weizmann.ac.il/fldbin/findex), predicts if a given protein sequence is intrinsically unfolded implementing the algorithm of Uversky and co-workers (*41*), which is based on the average residue hydrophobicity and net charge of the sequence (*39*).

*Expression and Purification of LEN.* A frozen stock of *Escherichia coli* JM83 cloned with the plasmid *pk*IVlen004, the expression system constructed by F. Stevens (*28*), was grown in a rich medium, and LEN was expressed as described previously (*29, 30*). The overexpressed protein LEN was purified using the procedure of Stevens et al. (*28*). Protein dialyzed against a 10 mM Tris buffer at pH 7.4 after sucrose and water extracts were pooled together, and then eluted through a HiTrip Q FF column (Pharmacia) to remove some protein impurities. After dialysis against a 10 mM acetate buffer at pH 4.0, the flow through from the HiTrip Q FF column was loaded onto a Hi Trip SP FF column (Pharmacia) and protein was eluted using a NaCl gradient from 0 to 200 mM over 30 min. The fractions were assayed by SDS gel electrophoresis, and the fractions containing the recombinant protein were pooled and concentrated by ultrafiltration using a membrane with a 3000 kDa cutoff (Amicon). The resulting protein solution was loaded onto a size-exclusion column [Sephacryl 200 (Pharmacia)] for further purification. Protein concentrations were measured via optical density at 280 nm using an extinction coefficient ($E_{0.1\%}$) of 1.71 calculated from the amino acid sequence. The concentration of the LEN stock solution was ~10 mg/mL. The purified LEN was stored in glass vials in 10 mM phosphate butter (pH 7.4) at 4 °C. The purity of the protein was assessed by SDS gel electrophoresis and by electrospray mass spectrometry.

*Oxidation of LEN by Hydrogen Peroxide.* The oxidation of LEN was induced by the incubation of a protein solution in the presence of 4 M GuHCl and 4% $H_2O_2$ at room temperature for 20 min. GuHCl and nonreacted peroxide were removed from the protein solution by dialysis against a 10 mM phosphate buffer solution at pH 7.4 (changing the buffer three times over 24 h). The extent of LEN oxidation was confirmed by mass spectrometry analysis (MicroMass Quattro II).

*In Vitro Fibril Formation Assays.* Amyloid fibrils and/or aggregates were grown from purified protein solutions in 10 mM phosphate buffer containing 100 mM NaCl. The proteins underwent an ultracentrifugation at 178000*g* on an Airfuge (Beckman) for 30 min to eliminate the preexisting aggregates before incubation under the desired conditions. Protein solutions with a concentration of 0.5 mg/mL (10 mM HCl and 100 mM NaCl) were stirred in 2 mL HPLC glass vials (Fisher) containing microstirring bars (8.5 mm, Fisher). Volumes ranged from 500 to 1000 $\mu$L. The stirring rate was ~600 rpm. LEN fibril formation was monitored using a fluorescence assay based on the enhanced fluorescence of the dye thioflavin T (ThT) on binding to amyloid fibrils (*42*). Rayleigh light scattering and fluorescence spectra were recorded using a SPEX/Jobin-Yvon Fluoromax-2 spectrofluorometer.

*Circular Dichroism Measurements.* Far-UV circular dichroism (CD) spectra were recorded on an AVIV model 62DC spectropolarimeter between 250 and 200 nm with a step size of 1.0 nm with an averaging time of 3 s and by collecting five repeat scans. A cell with a path length of 0.01 cm was used. Near-UV CD spectra were recorded from 320 to 250 nm using a cuvette with a path length of 1 cm. The protein concentration was kept at 0.5−1 mg/mL throughout these experiments. The background was subtracted from all the spectra, and the data were converted into mean residue ellipticities.

*Protein Stability toward GuHCl-Induced Unfolding.* The conformational stability of LEN at pH 7.4 (10 mM phosphate buffer) was assessed by measuring the intrinsic fluorescence using a FluoroMax-2 fluorescence spectrometer (Jobin Yvon-Spex) at 25 °C with a protein concentration of 0.1 mg/mL. Intrinsic fluorescence measurements were performed by recording the emission spectra between 305 and 450 nm, with an excitation wavelength of 295 nm. The samples were incubated in 10 mM phosphate buffer (pH 7.4) and varying amounts of GuHCl (0−5 M) for 1 h to make sure that the unfolding reaction reached equilibrium.

The fluorescence intensity and wavelength of emission maximum values were analyzed by a nonlinear least-squares method that fit to two-state unfolding model. The fraction unfolded ($F_u$) was calculated by using the equation

$$F_u = (y_f - y)/(y_f - y_u)$$

where $y_f$ and $y_u$ represent the intrinsic fluorescence of the folded and unfolded states, respectively, and $y$ represents the observed fluorescence at the given GuHCl concentration.

*Thioflavin T and ANS Fluorescence.* Fluorescence measurements were performed using a FluoroMax-2 fluorescence spectrophotometer (Jobin Yvon-Spex, Edison, NJ). ANS fluorescence was excited at 380 nm, and the emission spectra were recorded from 420 to 600 nm at 25 °C. In these experiments, the final concentrations of ANS and protein were 10 $\mu$M and 0.1 mg/mL, respectively. ThT fluorescence was excited at 450 nm, and the emission spectra were recorded from 465 to 560 nm. In these experiments, 10 $\mu$L protein solutions were added to 1.0 mL of the ThT solution (10 $\mu$M) before the measurements.

*Thin-Film-Attenuated Total-Reflectance Fourier Transform Infrared Spectroscopy (ATR-FTIR).* FTIR spectra of LEN were recorded on a ThermoNicolet Nexus 670 FTIR spectrophotometer from 4000 to 400 $cm^{-1}$ using a 2 $cm^{-1}$ resolution and an accumulation of 64 scans. Ten microliters of protein solutions of nonoxidized and MetO LEN were applied evenly on the surface of a germanium crystal and dried to form a hydrated thin film by being passed through a nitrogen stream. Background and water vapor subtractions were performed. Curve fitting of the amide I regions (raw spectra) was performed using Gaussian/Lorentzian functions (Grams). Second-derivative and Fourier self-deconvoluted spectra were used as a peak position guide for the curve fitting procedure.

*Transmission Electron Microscopy.* LEN aggregates were analyzed by EM. The stirred protein solutions were sampled at predetermined time points during the kinetic experiments by dropping 10 $\mu$L protein samples on Formarvar-coated copper grids. After the excess sample had been drained with filter paper, the grids were rinsed three times with water and air-dried. A freshly prepared 2% (w/v) uranyl acetate solution was then applied on the grids for 5 min. After the removal of the excess negative staining solution, the grids were air-dried again. Electron micrographs were collected using a JEOL JEM-100B microscope with a voltage accelerator of 80 kV. A magnification of 75000× was used.

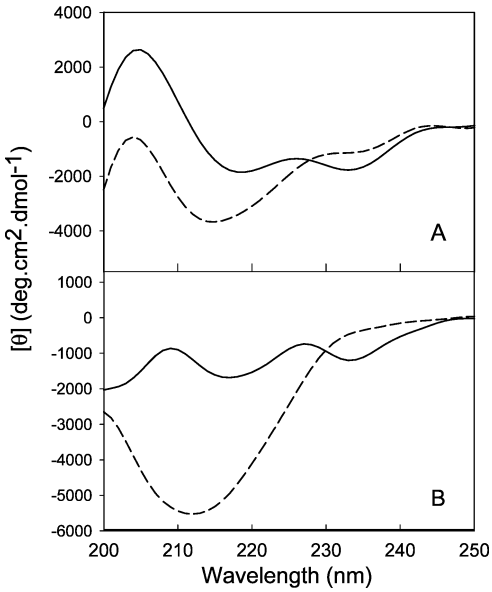


FIGURE 1: Comparison of the secondary structures of methionine-oxidized LEN and native LEN at neutral and acidic pH monitored by far-UV CD. (A) Far-UV CD spectra at pH 7.4 measured with a protein concentration of 1.0 mg/mL and a path length of 0.1 mm in 10 mM phosphate buffer at 25 °C. (B) Far-UV CD spectra at pH 2.0, measured with a protein concentration of 1.0 mg/mL and a path length of 0.1 mm in 10 mM phosphate buffer at 25 °C. The solid and dashed lines correspond to nonoxidized and MetO proteins, respectively.

## RESULTS

*In Vitro Oxidation of LEN.* There is one methionine ($Met^4$), two cysteine ($Cys^{23}$ and $Cys^{88}$), two tryptophan ($Trp^{35}$ and $Trp^{50}$), and nine tyrosine ($Tyr^{31}$, $Tyr^{38}$, $Tyr^{42}$, $Tyr^{55}$, $Tyr^{92}$, $Tyr^{93}$, $Tyr^{97}$, $Tyr^{98}$, and $Tyr^{102}$) residues in LEN, all of which are readily oxidized under the appropriate conditions. Among these residues, the methionine is the most easily oxidized to methionine sulfoxide, by two-electron oxidations induced by $H_2O_2$, among many other biological oxidants (*35*). Unexpectedly, the LEN was well-protected from oxidative modification, even being incubated in the presence of 4% $H_2O_2$ for 2 h at room temperature (data not shown). In the presence of 4 M GuHCl, where LEN was mostly unfolded, the methionine residue was oxidized to methionine sulfoxide (MetO) with 4% $H_2O_2$ after the incubation at room temperature for 20 min. The oxidation was confirmed by the increase in the molecular mass from 12636 to 12652 Da detected by mass spectrometric analysis. This 16 Da increase in the LEN mass was attributed to methionine oxidation (adding one oxygen atom).

*Changes in the Secondary Structure of LEN Induced by Methionine Oxidation.* LEN is a $\beta$-rich protein with a classical $\beta$-sandwich immunoglobulin fold (*27*). As shown in Figure 1, the far-UV CD spectrum of nonoxidized LEN under native conditions [10 mM phosphate buffer (pH 7.4)] was characterized by two minima (235 and 219 nm). The minimum at 219 nm is characteristic of $\beta$-structure, whereas a 235 nm minimum is attributed to the contribution of aromatic residues (tyrosine clusters) to the far-UV CD region (*43*). Methionine oxidation resulted in a significant increase in the degree of disorder in comparison with that of the nonoxidized protein. This was manifested by a noticeable shift of the 219 nm minimum to 214 nm accompanied by a dramatic increase in the negative ellipticity (Figure 1A). In addition, a substantial decrease in the negative ellipticity at 235 nm suggested that the environment of the aromatic residues in MetO LEN is more symmetric than that in the nonoxidized protein.

Substantial evidence supports the hypothesis that "pathological" or abnormal aggregation of LEN arises from a key partially folded intermediate precursor which is formed under mildly destabilizing conditions (pH 2 or 7 with some amount of detergent) (*29*). To characterize conformational changes induced in LEN by methionine oxidation, far-UV CD spectra of both nonoxidized and MetO LEN were recorded at pH 2.0, i.e., under conditions favoring fibril formation (*32*). As shown in Figure 1B, the far-UV CD spectrum of the nonoxidized protein measured at pH 2.0 was rather similar to that measured at pH 7.4, with a small decrease in the negative ellipticity at 235 nm. This reflected a slightly increased degree of disorder in the environment of the aromatic residues (tyrosine clusters), likely due to the partial unfolding of LEN at low pH. In MetO LEN, a significant increase in ellipticity at 212 nm, together with the complete disappearance of the 235 nm minimum, was observed, reflecting the noticeable rearrangement of $\beta$-structure and/or aromatic cluster.

The secondary structures of nonoxidized and MetO LEN in both neutral and acidic environments were further analyzed by hydrated thin-film ATR-FTIR. Figure 2 shows that the FTIR amide I spectrum of native LEN [10 mM phosphate buffer (pH 7.4)] possesses a main peak at 1637 $cm^{-1}$, reflecting the predominantly $\beta$-sheet structure. No dramatic changes in the FTIR spectra in the amide I region were observed at acidic pH (see Figure 2 and Table 1), which is consistent with the far-UV CD results. The detailed analysis of the secondary-derivative spectra revealed that the $\beta$-structure content increased slightly from 73.9% at pH 7.4 to 77.7% at pH 2, indicating a small structural reorganization (Table 1). Figure 2C and Table 1 show that the methionine oxidation induced a small decrease in the LEN $\beta$-structure content (from 73.9% in nonoxidized LEN to 65.1% in MetO LEN). When the pH was decreased to 2, the $\beta$-structure content of MetO LEN increased slightly compared to that at neutral pH (Table 1). However, the high degree of similarity of both spectra indicated the absence of the major changes in the secondary structure (cf. panels C and D of Figure 2). These observations suggested that the significant changes induced by methionine oxidation in the far-UV spectra of LEN should be attributed to the rearrangement of the tyrosine cluster and its environment, rather than to the secondary structure changes.

*Changes in Tertiary Structures of LEN Induced by Methionine Oxidation.* The near-UV CD spectra of nonoxidized and MetO LEN were recorded at pH 7.4 and 2.0 at 0.5 mg/mL (Figure 3). In the near-UV CD spectrum of native LEN, three maxima at 297, 289, and 280 nm were observed. The methionine oxidation of the protein resulted in a significant decrease in the intensities of these peaks. However, they were still observed at pH 7.4. This indicated that although the oxidized protein lost the majority of its tertiary structure, some residual tertiary structure might be present in MetO LEN. At pH 2.0, i.e., under conditions promoting LEN fibrillation, nonoxidized LEN was characterized by the pronounced near-UV CD spectrum, which was rather similar

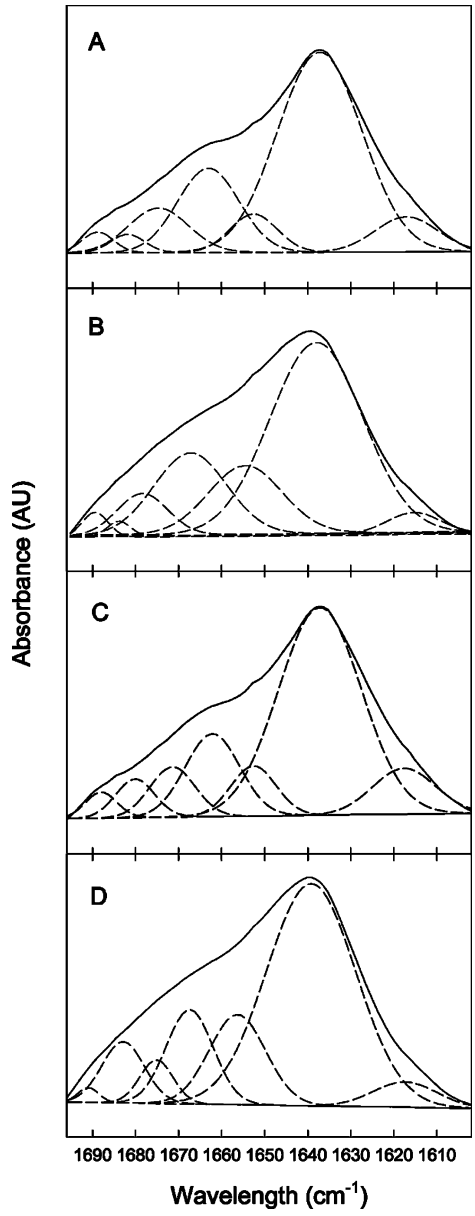


FIGURE 2: Amide I regions of the FTIR spectra of methionine-oxidized and nonoxidized LEN at pH 7.4 and 2.0 (10 mM phosphate buffer): (A) LEN at pH 7.4, (B) MetO LEN at pH 7.4, (C) LEN at pH 2.0, and (D) MetO LEN at pH 2.0. The solid lines represent the raw ATR-FTIR spectra, and the dashed lines represent the curve-fitted components used for secondary structure analysis.

to that measured at pH 7.4 (Figure 3B). This indicated that the tertiary structure of LEN, being slightly modified, was still maintained under these conditions. However, the near-UV CD spectrum of MetO LEN was featureless, suggesting the complete loss of the tertiary structure at pH 2.0.

Analysis of the near-UV CD, far-UV CD, and FTIR spectra revealed that the methionine oxidation induced significant structural alterations in LEN. In fact, MetO LEN was characterized by a well-developed nativelike secondary structure, whereas its tertiary structure was almost completely diminished even at neutral pH. These differences between the nonoxidized and oxidized LEN became even more evident at pH 2.0, where nonoxidized protein preserved the majority of its native structure, whereas MetO LEN completely lost its tertiary structure while still preserving nativelike secondary structure. This strongly suggested that

Table 1: Secondary Structure Content of LEN[a]

| | peak position ($cm^{-1}$) | secondary structure assignment | area under the curve (%) |
|---|---|---|---|
| LEN at pH 7.4 | 1688 | turns/loops | 2.56 |
| | 1682 | $\beta$-sheet | 2.53 |
| | 1675 | $\beta$-sheet | 9.08 |
| | 1663 | turns/loops | 17.20 |
| | 1653 | turns/loops | 6.30 |
| | 1637 | $\beta$-sheet | 54.83 |
| | 1617 | $\beta$-sheet | 7.50 |
| MetO LEN at pH 7.4 | 1689 | turns/loops | 0.07 |
| | 1683 | $\beta$-sheet | 0.34 |
| | 1677 | $\beta$-sheet | 6.50 |
| | 1667 | turns/loops | 16.33 |
| | 1654 | turns/loops | 18.65 |
| | 1638 | $\beta$-sheet | 55.79 |
| | 1615 | $\beta$-sheet | 2.33 |
| LEN at pH 2.0 | 1688 | turns/loops | 1.47 |
| | 1680 | $\beta$-sheet | 3.88 |
| | 1671 | $\beta$-sheet | 6.57 |
| | 1662 | turns/loops | 14.34 |
| | 1654 | turns/loops | 6.56 |
| | 1637 | $\beta$-sheet | 58.59 |
| | 1617 | $\beta$-sheet | 8.59 |
| MetO LEN at pH 2.0 | 1691 | turns/loops | 0.81 |
| | 1682 | $\beta$-sheet | 7.33 |
| | 1675 | $\beta$-sheet | 4.8 |
| | 1667 | turns/loops | 12.58 |
| | 1656 | turns/loops | 14.36 |
| | 1639 | $\beta$-sheet | 56.35 |
| | 1618 | $\beta$-sheet | 4.50 |

[a] From hydrated thin-film ATR-FTIR spectra at 25 °C.

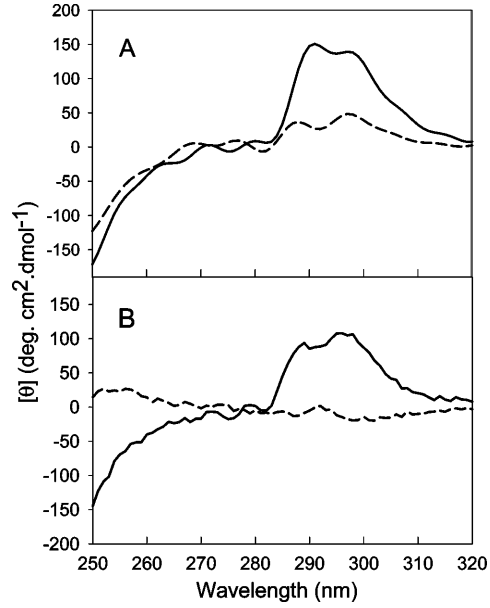


FIGURE 3: Methionine oxidation-induced changes in tertiary structures monitored by near-UV CD spectra. (A) Near-UV CD spectra at pH 7.4 measured with a protein concentration of 1.0 mg/mL and a path length of 1.0 cm in 10 mM phosphate buffer at 25 °C. (B) Near-UV CD spectra at pH 2.0 measured with a protein concentration of 1.0 mg/mL and a path length of 1.0 cm in 10 mM phosphate buffer at 25 °C. The solid and dashed lines correspond to nonoxidized and MetO proteins, respectively.

methionine oxidation induced transformation of LEN into a molten globule-like conformation, which is a compact denatured state characterized by a nativelike secondary structure and a high affinity for the hydrophobic fluorescent probe ANS (*44*).

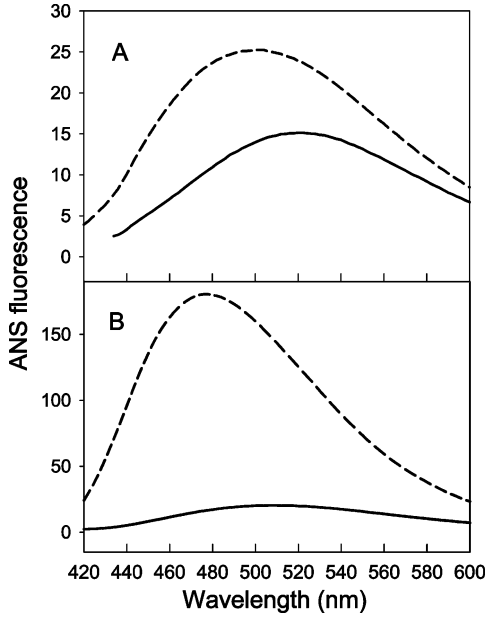


FIGURE 4: Comparison of ANS binding capabilities of nonoxidized and methionine-oxidized LEN at neutral and acidic pH. ANS fluorescence measurements were performed using an excitation wavelength of 380 nm and recording the emission spectra from 420 to 600 nm at 25 °C by adding 10 $\mu$M ANS to 1.0 mL of 0.1 mg/mL protein solutions at pH 7.4 (A) and pH 2.0 (B). The solid and dashed lines correspond to the nonoxidized and MetO proteins, respectively.

*Changes in Interaction of LEN with ANS Induced by Methionine Oxidation.* ANS fluorescence is frequently used to probe protein conformational reorganizations associated with the changes in the solvent exposure of hydrophobic regions (*45*), usually observed upon partial protein unfolding (*45*). Therefore, this technique is frequently used to detect the formation of molten globule-like species (*45*). Both an increase in the fluorescence intensity and a decrease in the $\lambda_{max}$ values (blue shift) are usually observed upon binding of ANS to exposed hydrophobic clusters. As shown in Figure 4, the ANS spectrum in the presence of nonoxidized LEN at neutral pH was characterized by a $\lambda_{max}$ at ~524 nm, indicating the absence of ANS binding to the protein under these conditions. ANS fluorescence in the presence of the methionine-oxidized protein, however, possessed a $\lambda_{max}$ at approximately 495 nm and enhanced intensity, indicating noticeable ANS binding to the protein. This gave further support to the hypothesis that the methionine oxidation of LEN induced the structural rearrangement of the protein into the molten globule-like conformation, where the nativelike secondary structure was preserved, whereas the level of tertiary structure was diminished and the hydrophobic core became exposed to the solvent.

At pH 2.0, some enhancement of the ANS binding to the nonoxidized LEN was observed as indicated by the $\lambda_{max}$ blue shift from 520 to 500 nm, accompanied by a slight increase in ANS fluorescence intensity. This suggested that the hydrophobic clusters were still mostly buried in the core of LEN, though a small exposure took place. However, the methionine-oxidized LEN at low pH exhibited a very high affinity for ANS, as indicated by the $\lambda_{max}$ at 475 nm and significantly enhanced fluorescence intensity. In combination with other spectroscopic data, this indicated that the decrease in pH completed the structural transformation of MetO LEN into the molten globule.

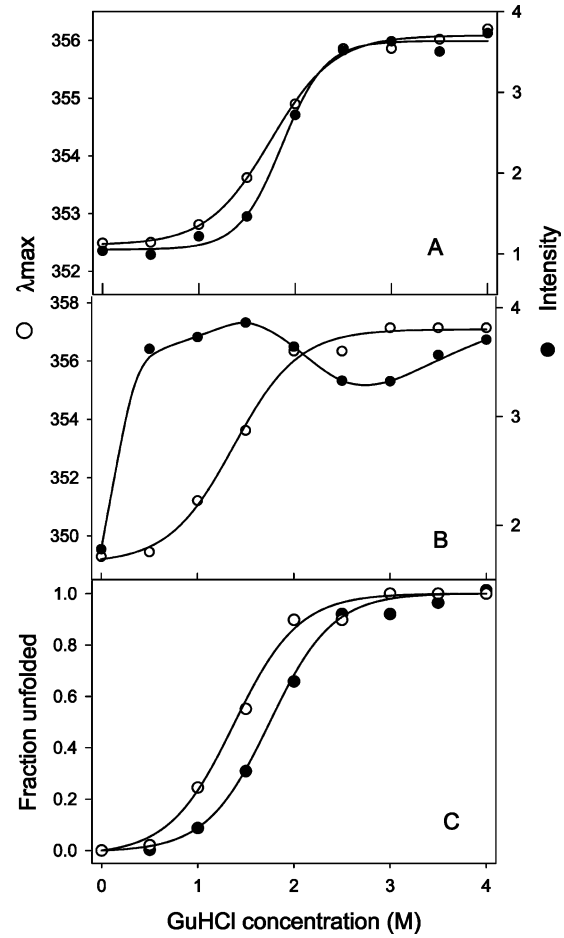


FIGURE 5: Change in the conformational stability of LEN induced by methionine oxidation measured by intrinsic fluorescence in the presence of various concentrations of GuHCl. Panels A (nonoxidized LEN) and B (MetO LEN) show the GuHCL unfolding curves monitored by Trp fluorescence intensity (●) and $\lambda_{max}$ (○). (C) Comparison of fraction unfolded curves for the nonoxidized LEN (●) and MetO LEN (○) derived from the Trp fluorescence $\lambda_{max}$ values in the presence of various concentrations of GuHCl.

*Changes in the Trp Environment Induced by Methionine Oxidation.* The tryptophan fluorescence is known to be very sensitive to subtle structural reorganizations in the vicinity of a chromophore. The intrinsic fluorescence of LEN is determined by the presence of two tryptophan residues, $Trp^{35}$ and $Trp^{50}$. In the native state, $Trp^{35}$ is buried in the hydrophobic core of the protein and is completely quenched by the spatial proximity of the $Cys^{23}-Cys^{88}$ disulfide bridge, whereas $Trp^{50}$ is significantly solvent-exposed (*27*) (see Figure 6A). Therefore, the intrinsic fluorescence of native LEN is mostly determined by the solvent-exposed $Trp^{50}$, which is indicated by the $\lambda_{max}$ of 352.5 nm at pH 7.4 in the absence of GuHCl (Figure 5). The intrinsic fluorescence of MetO LEN was characterized by a $\lambda_{max}$ of 349 nm at pH 7.4 in the absence of GuHCl. This suggested that either $Trp^{50}$ was more buried in MetO LEN than in the native protein or the spatial positions of $Trp^{35}$ and the $Cys^{23}-Cys^{88}$ disulfide bridge were changed, leading to less effective quenching. The fact that the Trp fluorescence intensity of MetO LEN was almost 2-fold higher than that of the nonoxidized protein supported the hypothesis that changes in intrinsic fluores-

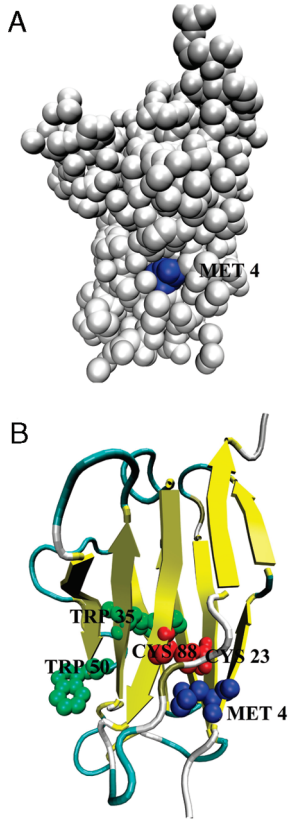


FIGURE 6: Spatial pattern of LEN. (A) Surface of the protein. Met[4] is colored blue. (B) Cartoon diagram of the protein. Localization of Met[4] (blue), Trp[35] (green), Trp[50] (light green), and the disulfide bridge between Cys[23] and Cys[88] (red) shown as spheres. This figure was constructed on the basis of the LEN structure given in Protein Data Bank entry 1LVE (*27*). The drawing was generated with VMD (*58*).

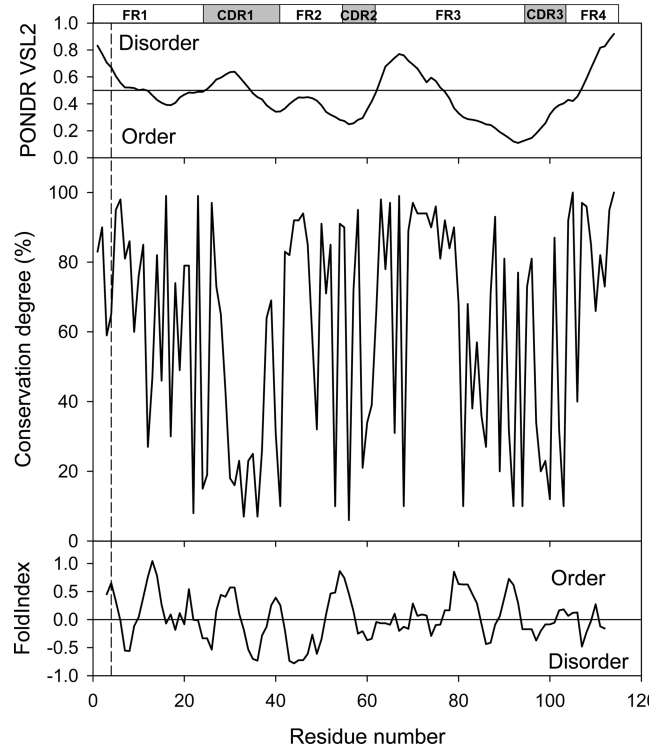


FIGURE 7: Computational analysis of the LEN sequence. The middle plot illustrates the conservation of the LEN sequence based on the BLAST analysis of the Swiss-Prot database. Top and bottom panels represent the results of the LEN analysis by the PONDR VSL2 and FoldIndex algorithm, respectively. The dashed vertical line illustrates the Met[4] position. Bars on the top of the figure represent the localization of four framework regions (FR1, FR2, FR3, and FR4) as well as the localization of three complementarity-determining regions (CDR1, CDR2, and CDR3).

cence were due to the changes in the Trp[35] environment. This hypothesis was further supported by the almost complete elimination of the characteristic features in the LEN near-UV CD spectrum induced by the methionine oxidation (see Figure 3).

*Changes in Conformational Stability Induced by Methionine Oxidation.* The GuHCl-induced unfolding of LEN and MetO LEN at pH 7.4 was studied by characteristic changes in intrinsic fluorescence. Figure 5A shows that GuHCl-induced unfolding of native LEN was accompanied by a significant increase in the Trp fluorescence intensity, and by the shift of the $\lambda_{max}$ from 352.5 to 356 nm. Changes in these two parameters occurred almost simultaneously, being characterized by a $C_{1/2}$ of ~1.8 M GuHCl. These spectral perturbations indicated that Trp[35], buried in the hydrophobic core of the native protein, moved away from the Cys[23]−Cys[88] disulfide bridge and became solvent-exposed. In MetO LEN, the increase in the GuHCl concentration was accompanied by a red shift from 349 to 358 nm ($C_{1/2}$ ~ 1.2 M GuHCl) and a set of complex changes in the fluorescence intensity, which first sharply increased almost 2-fold ($C_{1/2}$ ~ 0.2 M GuHCl) and then showed sigmoid changes with a $C_{1/2}$ of ~2.0 M GuHCl (Figure 5B). Finally, Figure 5C shows that methionine oxidation resulted in the noticeable destabilization of a protein.

*Analysis of the Met[4] Local Environment.* Analysis of the local environment of the single methinione residue of LEN (Met[4]) revealed that although it is located in the periphery of the hydrophobic core of the macromolecule (Figure 6B), the density of its microenvironment is rather high. In fact, it contains 10 side chains (including Val[3], Thr[5], Cys[23], Lys[24], Ser[25], Leu[33], Cys[88], Gln[90], Ser[97], and Gly[99]) and 22 atoms (within a 4 Å sphere). Furthermore, Met[4] is rather close to the disulfide bond (5.25 Å), being 15 Å from Trp[35] (Figure 6A). Therefore, the folded structure of this LC includes the snug-fitting environment for the buried Met side chain and hence protects it from $H_2O_2$ (despite the small size of the OH radical). However, the addition of the oxygen to the Met[4] sulfur presumably radically breaks the snugness of this burial, significantly loosening the structure of the entire protein. In fact, in the proximity of Met[4], there are residues from both N- and C-termini as well as some residues from the middle part of LEN. In agreement with this hypothesis, our experimental data suggest that Trp[35] and the disulfide bond move apart in response to Met[4] oxidation.

Interestingly, BLASTing (*46*) LEN against the Swiss-Prot database revealed that Met[4] is rather conserved (Figure 7, central plot). In fact, this residue possesses a degree of conservation of 65%, being conservatively substituted with either Leu (33%) or Ile (2%). Earlier, the Met[4] to Leu (M[4]L) substitution in the core of LEN was shown to result in a noticeable stabilization of this domain (by 1.0 kcal/mol) (*25*). A similar stabilizing effect was reported for the M[4]L mutation in a murine $F_v$ fragment (*47*). It has been proposed that the leucine residue, being completely buried, occupies the same space as the methionine in wild-type LEN (*25*). In the interior of a protein, a Met-to-Leu substitution is expected to stabilize

the protein by ~1.4 kcal/mol if it does not introduce strain into the structure (*48*). The fact that the $M^4L$ substitution in LEN produced comparable stabilization (1.0 kcal/mol) suggested that it did not introduce noticeable alteration into the packing of the hydrophobic core.

*Predicted Flexibility of the Met⁴-Containing N-Terminal Fragment.* Additional clues about the conformational behavior of nonoxidized and MetO LEN can be derived from the analysis of its intrinsic disorder propensities. Recently, protein flexibility and especially its extreme case, intrinsic protein disorder, attracted considerable attention from researchers. Numerous recent studies and reviews clearly reflect the growing interest in the intrinsically disordered proteins. A special database, DisProt, has been created for the collection of structural and functional information about these proteins (*49*). In part, this stably increasing interest is due to the fact that these flexible regions are crucial for many nonenzymatic protein functions. Statistical analyses of amino acid composition, flexibility, hydropathy, charge, coordination number, and several other factors have revealed that sequences of intrinsically disordered (and thus highly flexible) proteins, or regions of proteins, are significantly different from intrinsically ordered (regions of) proteins. An intrinsically disordered region is characterized by a low level of sequence complexity coupled with a compositional bias; a low content of order-promoting residues, such as bulky hydrophobic amino acids (V, L, I, M, F, W, and Y) normally forming the core of a folded globular protein, and cysteine; and a high proportion of polar, charged, and structure-breaking amino acids (Q, S, P, E, K, and, less often, G and A) promoting disorder (*40, 50*). These differences were utilized in developing a number of disorder predictors, many of which can be accessed at the DisProt database (*49*). The results of application of two of these, PONDR VSL2 (*38*) and FoldIndex (*39*), to the LEN sequence are shown in the top and the bottom panels of Figure 7, respectively. High PONDR VSL2 scores for the N-terminal fragment of LEN indicate that this protein segment is predisposed to being flexible. On the other hand, FoldIndex predicts this fragment to be ordered due to the relatively high content of the hydrophobic residues (Figure 7). Taken together, these results suggest that ~20 N-terminal residues of LEN are likely in the metastable folded state, which easily can be affected by some environmental factors, e.g., by $Met^4$ oxidation, which make this residue more polar.

*Effect of Methionine Oxidation on LEN Aggregation Behavior.* Changes in the thioflovin T (ThT) fluorescence were used to monitor the kinetics of fibril formation, whereas Rayleigh light scattering was utilized to follow the formation of large aggregates. As shown in Figure 8A, incubation of the nonoxidized LEN produced a sigmoid increase in ThT fluorescence intensity with a lag time of 10 h. The slight increase in the magnitude of the signal during the lag time reflected the formation of oligomeric species with some affinity for ThT (*29–31*). The large-scale changes in ThT fluorescence occurred simultaneously with the increase in Rayleigh light scattering (cf. panels A and B of Figure 8), indicating the formation of large fibrillar aggregates. The fibrils formed after the exponential growth phase (after incubation for 50 h) were visualized by negatively stained transmission electron microscopy (Figure 9C).

In the case of MetO LEN, the fast formation of aggregates

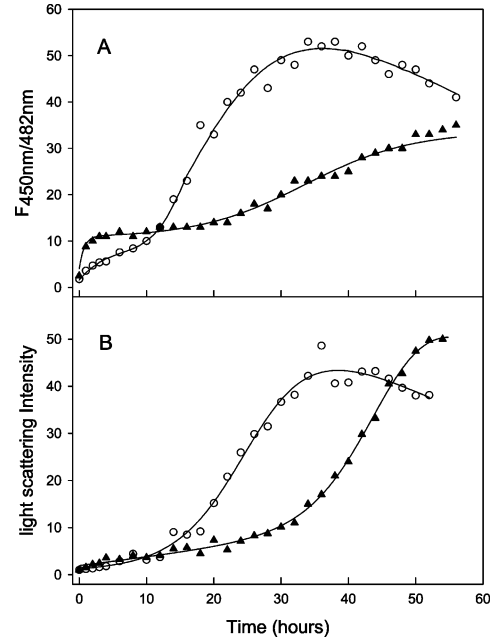


FIGURE 8: Kinetics of the aggregation of nonoxidized LEN (○) and MetO LEN (▲) monitored by thiflovin T (ThT) (A) and light scattering (B). The protein solutions were stirred at 0.5 mg/mL, 37 °C, and 600 rpm in phosphate buffer with 100 mM NaCl.

was observed at the beginning of the incubation period (in 5 h) as indicated by the increase in both ThT fluorescence (Figure 8A) and Rayleigh light scattering (Figure 8B). The formation of amorphous aggregates was also confirmed by EM (Figure 9A). Although the lag time was longer than that of the nonoxidized protein, the formation of fibrils after the prolonged incubation of MetO LEN was detected by ThT fluorescence (Figure 8A) and EM image (Figure 9B). The significantly lower intensity of the ThT fluorescence indicated that a smaller amount of fibrils was formed in the methionine-oxidized sample. This conclusion was also confirmed by the EM analysis (cf. panels B and C of Figure 9).

*Changes in the Secondary Structure of Nonoxidized and MetO LEN during Incubation.* Far-UV CD spectra of both nonoxidized and MetO LEN were recorded during the early stages of aggregation induced by incubation with stirring at pH 2.0. In the first 10 h of incubation, which was the lag time of fibrillation, a slight increase in ellipticity at 217 nm was observed, indicating the existence of a slight conformational adjustment of LEN during the nucleation period. Simultaneously with the significant increase in the ThT signal, the ellipticity of the nonoxidized protein dramatically increased, and the shape of the far-UV CD spectrum changed, reflecting the conformational reorganization to a typical $\beta$-sheet-enriched structure during fibril elongation (Figure 10A,B).

At the beginning of the incubation, MetO LEN exhibited immediate changes in both the spectral intensity and the minimum position. The increase in ellipticity and shift of the minimum position from 212 to 210 nm occurred in the first 6 h of the incubation. However, no evidence of fibril formation was found during this time period, suggesting that the observed spectral changes reflected the conformational reorganization during oligomerization and amorphous aggregate formation (Figure 10C,D). Interestingly, both ellipticity and minimum position in the far-UV CD spectra of

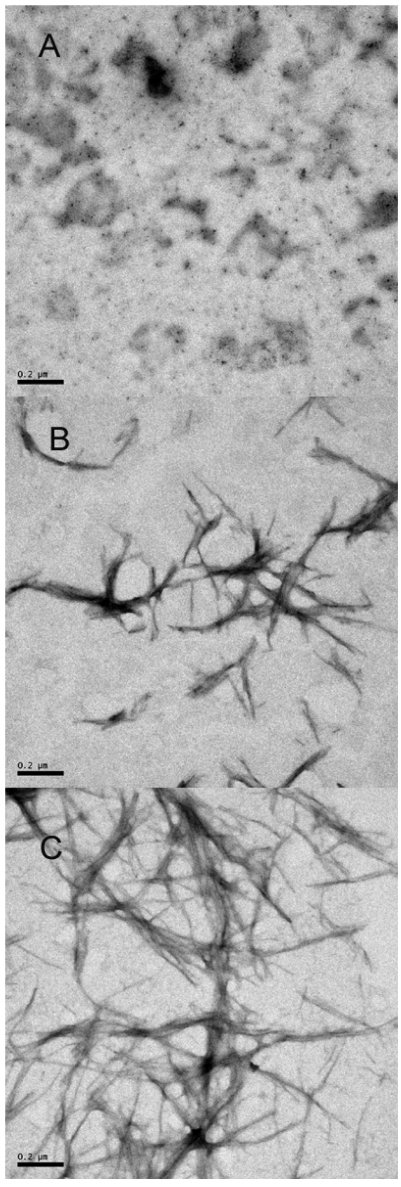


FIGURE 9: Negatively stained transmission electron micrographs of aggregates of representative nonoxidized and MetO LEN. (A) MetO LEN after incubation for 5 h. (B) MetO LEN after incubation for 50 h. (C) Nonoxidized LEN after incubation for 50 h.

MetO LEN were not changed during the incubation between 6 and 20 h, followed by another phase in which the continuous increase in negative ellipticity was accompanied by a shift in minimum position from 210 to 217 nm, indicating the formation of fibrils.

The secondary structure of LEN and MetO LEN during aggregation was further analyzed by hydrated thin-film ATR-FTIR (Figure 11). Initially, the major peak in both LEN and MetO LEN FTIR amide I spectra was observed at 1638 $cm^{-1}$, which is typical for $\beta$-proteins. In the first 12 h of incubation, which was within the lag time of LEN fibrillation, there was an only slight change in the spectrum of nonoxidized LEN, reflecting the lack of dramatic structural reorganization (Figure 11A). After the sample had been stirred for 34 h, a significant shift of the peak maximum toward the lower wave numbers (1630 $cm^{-1}$) was observed concomitantly with a significant decrease in the intensity in the 1660−1640 $cm^{-1}$ region. These spectral changes reflected the structural reorganization of LEN to more ordered $\beta$-structure (i.e., to so-called aggregation $\beta$-structure), indicating the formation of fibrils.

In contrast to the nonoxidized LEN, structural reorganization of MetO LEN occurred in the first 2 h of incubation. This was indicated by the peak maximum shift from 1638 to 1630 $cm^{-1}$ (Figure 11B). This structural reorganization was accompanied by the oligomer and amorphous aggregate formation, as indicated by the ThT/light scattering assay (Figure 8). The continuous right shift of the peak maximum (toward lower wavenumbers) was observed during the 12 h of incubation with stirring, likely reflecting further protein association. The FTIR amide I spectrum of MetO LEN after incubation for 34 h exhibited a peak maximum at 1630 $cm^{-1}$ with decreased intensity in the vicinity of 1660−1640 $cm^{-1}$, indicating the formation of fibrils. This was also confirmed by the ThT assay (Figure 8) and electron microscopy (Figure 9).

ANS fluorescence was also used to probe protein conformational changes during the association−aggregation processes of nonoxidized and MetO LEN (see Figure 12). In this study, 10 $\mu$M ANS was used, as at this concentration no binding of ANS to wild-type LEN was detected, but there was a significant ANS binding to MetO LEN as shown in Figure 4. At the beginning of the nonoxidized LEN incubation, both an increase in the ANS fluorescence intensity and a blue shift of its $\lambda_{max}$ were observed. Importantly, the changes in the ANS $\lambda_{max}$ took place prior to the major changes in ThT fluorescence. This indicated a structural transformation into a conformation with the solvent-exposed hydrophobic clusters. In the case of MetO LEN, no changes in $\lambda_{max}$ were detected, but an immediate increase in the ANS fluorescence intensity at the beginning of the incubation was found, suggesting that the aggregates of MetO LEN had a more solvent-exposed hydrophobic area accessible to ANS (Figure 12).

## DISCUSSION

Pathological outcomes of aggregation, fibril formation, and/or aggregate/fibril deposition are different for different diseases, ranging from the targeted neuron death in the highly localized brain regions in neurodegenerative diseases and ending with the gross tissue disruption by large masses of fibrils in classical peripheral amyloidoses. However, a common molecular mechanism is believed to underlie the fibril formation process associated with various amyloidosis diseases. The hypothesis that fibril formation arises from partially folded intermediates has usually been favored (*5, 7, 12, 51*). This hypothesis is supported by the following facts.

(i) The fibrils from different pathologies are rather similar and possess a number of common structural features, including a twisted, ropelike structure and a cross-$\beta$-sheet structure, where continuous $\beta$-sheets are formed with $\beta$-strands running perpendicular to the long axis of the fibrils (*52*).

(ii) Despite similarities characteristic of amyloid fibrils, more than 20 proteins known to be involved in deposition diseases are structurally unrelated (*7*). Prior to fibrillation, amyloidogenic proteins may be rich in $\beta$-sheet, α-helix, and $\beta$-helix or contain both α-helices and $\beta$-structure; they may be well-folded globular proteins with unique three-dimen-

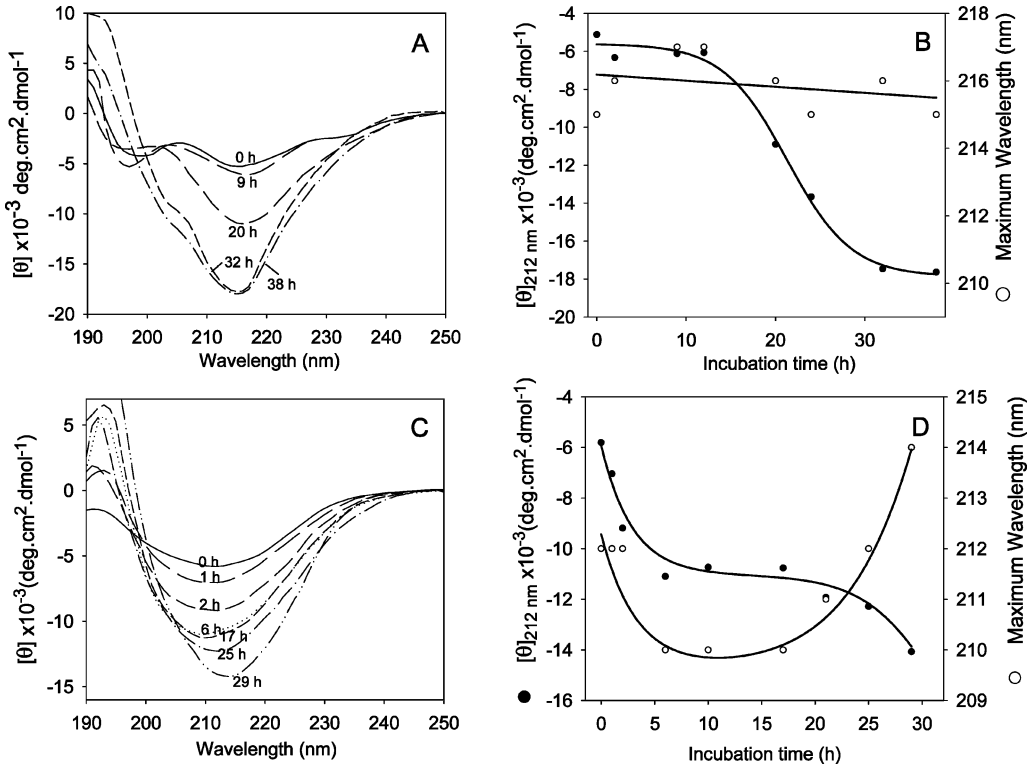


FIGURE 10: Comparison of the kinetics of the secondary structure changes of nonoxidized and MetO LEN during incubation monitored by far-UV circular dichroism. The protein solutions were stirred at 600 rpm and 37 °C in 10 mM phosphate buffer in the presence of 100 mM NaCl. (A) Spectra of nonoxidized LEN at the time points of incubation. (B) Analysis of transitions of both the ellipticity and the positions of minimum derived from panel A. (C) Spectra of methionine-oxidized LEN at the time points of incubation. (D) Transitions of both the ellipticity and the positions of minima derived from panel C.

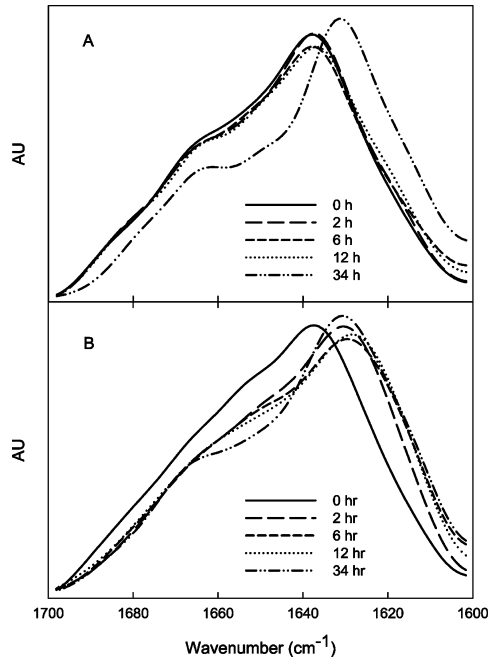


FIGURE 11: Amide I region of the FTIR spectra of LEN (A) and methionine-oxidized LEN (B) solutions at pH 2 (20 mM HCl and 100 mM NaCl) as a function of stirring time: 0 (—), 4 (– – –), 6 (---), 12 (•••), and 34 h (•••••). LEN solutions were stirred at 0.5 mg/mL, 37 °C, and 600 rpm.

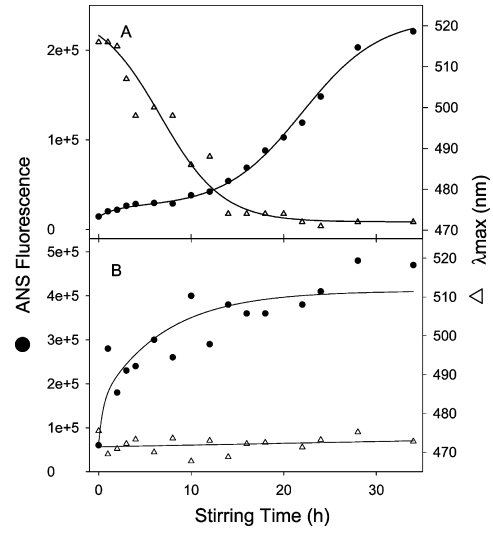


FIGURE 12: Comparison of the conformational changes in the nonoxidized and MetO LEN during incubation monitored by ANS fluorescence. The protein solutions were stirred at 600 rpm and 37 °C in 10 mM phosphate buffer in the presence of 100 mM NaCl. The transitions of ANF fluorescence intensity and maximum emission wavelength for nonoxidized LEN (A) and MetO LEN (B) were plotted vs incubation time.

sional structures or be intrinsically unstructured (*5*). This suggests that there might be a unifying mechanism of protein fibrillation that involves structural transformation of a polypeptide chain into a partially folded conformation, which originates due to the partial destabilization of physiologically folded globular proteins (*3–13*), or because of the partial folding of natively unfolded (or intrinsically disordered) proteins (*5, 14–16, 51*). Presumably, such a partially unfolded conformation enables specific intermolecular interactions, including electrostatic attraction, hydrogen bonding, and hydrophobic contacts, which are necessary for oligomerization and fibrillation.

Furthermore, fibril formation has been hypothesized to occur stepwise, a slow phase of nuclei formation preceding a relatively fast elongation−growth phase (*14, 53*). However, both the triggering factors and the mechanisms involved in the abnormal formation of in vivo insoluble fibrillar aggregates from soluble proteins are poorly understood (*54*).

The facts that the benign light chain domain LEN with no sign of renal dysfunction or amyloidosis in a patient suffering from multiple myeloma may still form fibrils under destabilizing conditions and the fact that its molecular analogue SMA, being only eight residues different from LEN, is an amyloidogenic protein suggest that some environmental factors could play a role in its fibrillation.

*LEN Oxidation.* Oxidative damage, probably through the intervention of various ROS, is one of the contributing factors in amyloid disease pathogenesis. The only methionine, which is located in the N-terminal part of the LEN amino acid sequence, is the most readily oxidized side chain. Given that mildly destabilizing conditions can lead to light chain aggregation, we oxidized LEN by adding hydrogen peroxide and studied the effect of methionine oxidation on protein structural properties, conformational stability, and aggregation. Surprisingly, the protein was well-protected from oxidation by $H_2O_2$ in its native state under physiological conditions. Two mechanisms can contribute to the observed high resistance toward the methionine oxidation: compactness/rigidity of a native structure and LEN dimerization. The analysis of the crystal structure (Protein Data Bank entry 1lve) revealed that the methionine residue is not located at the dimer interface, being deeply buried in the hydrophobic core of LEN. Thus, it is likely that this core location of methionine protects it from being oxidized.

However, in the presence of 4 M GuHCl, 4% hydrogen peroxide was able to add one oxygen atom to the protein molecule, which was confirmed by mass spectrometry. The addition of 4 M GuHCl resulted in complete LEN unfolding and dissociation of its dimers. We believe that the mentioned oxygen addition was due to the oxidation of the methionine residue.

*Conformational Modification Induced by Methionine Oxidation.* It is recognized that mildly destabilizing conditions such as 4 M urea, 2 M GuHCl, or pH 2.0 are necessary for LEN to form fibrils in vitro on a reasonable time scale. However, it is unknown what triggers the light chain fibrillation in vivo under physiological conditions. Though in light chain amyloidosis the most affected organ is the kidneys, where the pH is lower than the physiological pH, it is still not low enough to induce fibril formation found in in vitro experiments (*32*). Furthermore, the fact that several organs other than the kidneys are involved in the light chain amyloidosis also indicates that the acidic pH may not be the triggering factor to initiate the light chain fibrillation in vivo. On the other hand, some intramolecular modifications, such as point mutations or oxidative modifications, can decrease the conformational stability of a light chain and therefore promote its aggregation and fibrillation.

Data presented in this paper show that methionine oxidation of LEN has a significant effect on its structural properties, conformational stability, and propensity to aggregate. Although no noticeable changes in secondary structure were detected in MetO LEN in comparison with the nonoxidized protein under both physiological and acidic conditions, the far-UV and near-UV CD spectra indicated that a significant alteration of the tertiary structure took place upon oxidation. Overall, spectroscopic analysis revealed that MetO LEN possessed many features of the molten globule, including nativelike secondary structure, a lack of tertiary structure, and a high affinity for ANS. In addition, oxidation induced a decrease in the stability against GuHCl unfolding. All these factors can facilitate MetO LEN aggregation.

*Oxidized and Nonoxidized LEN Aggregation and Light Chain Deposition Diseases.* Overall, the results of our analysis show that the nonoxidized and MetO LEN have different aggregation pathways. Nonoxidized LEN forms soluble oligomers without significant structural reorganization. Earlier, it has been established that these rapidly formed soluble oligomers are off the LEN fibrillation pathway (*31*). Furthermore, although most of the protein was present in these off-pathway intermediates at early aggregation stages, eventually all the protein forms fibrils. A structural rearrangement from the non-fibril-prone off-pathway oligomers to a more fibril-prone species was analyzed by a variety of techniques (*31*). These analyses revealed the existence of dramatic structural changes within the soluble oligomers and suggested that fibrils were formed from the oligomers containing a less stable conformation of LEN, either directly or via dissociation (*31*).

In the case of MetO LEN, the aggregation started with a significant structural rearrangement, leading to the formation of insoluble amorphous aggregates, which inhibited MetO LEN fibrillation. This difference in aggregation behavior is determined by the structural alterations induced by methionine oxidation. In fact, MetO LEN was in a molten globule-like conformation even at neutral pH and was further destabilized at pH 2.0. Although the oxidized protein aggregated essentially faster than the nonoxidized LEN, the molten globule-like conformation of MetO LEN described in this paper seems to represent a species located off the fibrillation pathway.

It was observed that the morphology of light chain deposits varies in various light chain deposition diseases. In AL amyloidosis, which is the most common form of systemic amyloidosis, the amyloid fibrils derived from the light chain are the dominant proteinaceous deposits. LCDD, however, is the light chain deposition disease, where the amorphous deposits are found associated with the basement membranes (*17, 55*). Occasionally, patients may present both AL and LCDD pathologies that originated from the fibrillar and amorphous deposition of the same variable domain of the light chain ($V_L$), sometimes in the same tissue (*56*). Some other deposit morphologies are present in other light chain deposition diseases. For example, an amorphous cast was composed of the light chain in myeloma cast nephropathy and light chain crystals in Fanconi's syndrome. As reported previously (*30, 31*), in vitro studies of LEN and SMA aggregation revealed that the light chains tend to form fibrils from their partially unfolded states, whereas under mild denaturing conditions, where the light chain is in its nativelike intermediate, the protein readily forms amorphous aggregates (*57*). In our study, we showed that the methionine oxidation of LEN induced amorphous aggregation and partially inhibited protein fibrillation. During the early stage of aggregation, the rapid formation of molten globule-like oligomers, which are different from the profibrillation species

formed during the early stage of nonoxidized protein fibrillation, blocks the fibrillation pathway favoring amorphous aggregate formation. Therefore, these in vitro observations, taken together with the data on morphologically different proteinaceous deposition in various light chain deposition diseases, suggest that the multiple morphologies of light chain deposition could result from multiple factors, both intramolecular and external.

## ACKNOWLEDGMENT

We express our deepest gratitude to Alexey Uversky for carefully reading and editing the manuscript.

## REFERENCES

1. Glenner, G. G. (1980) Amyloid deposits and amyloidosis. The $\beta$-fibrilloses (first of two parts). *N. Engl. J. Med. 302*, 1283–1292.
2. Sipe, J. D. (1992) Amyloidosis. *Annu. Rev. Biochem. 61*, 947–975.
3. Uversky, V. N.; Talapatra, A.; Gillespie, J. R.; Fink, A. L. (1999)Protein deposits as the molecular basis of amyloidosis. I. Systemic amyloidoses. *Med. Sci. Monit. 5*.
4. Uversky, V. N., Talapatra, A., Gillespie, J. R., and Fink, A. L. (1999) Protein Deposits As the Molecular Basis of Amyloidosis. II. Localized Amyloidosis and Neurodegenerative Disorders. *Med. Sci. Monit. 5*, 1238–1254.
5. Uversky, V. N., and Fink, A. L. (2004) Conformational constraints for amyloid fibrillation: The importance of being unfolded. *Biochim. Biophys. Acta 1698*, 131–153.
6. Kelly, J. W. (1998) The alternative conformations of amyloidogenic proteins and their multi-step assembly pathways. *Curr. Opin. Struct. Biol. 8*, 101–106.
7. Dobson, C. M. (1999) Protein misfolding, evolution and disease. *Trends Biochem. Sci. 24*, 329–332.
8. Bellotti, V., Mangione, P., and Stoppini, M. (1999) Biological activity and pathological implications of misfolded proteins. *Cell. Mol. Life Sci. 55*, 977–991.
9. Rochet, J. C., and Lansbury, P. T., Jr. (2000) Amyloid fibrillogenesis: Themes and variations. *Curr. Opin. Struct. Biol. 10*, 60–68.
10. Lansbury, P. T., Jr. (1999) Evolution of amyloid: What normal protein folding may tell us about fibrillogenesis and disease. *Proc. Natl. Acad. Sci. U.S.A. 96*, 3342–3344.
11. Fink, A. L. (1998) Protein aggregation: Folding aggregates, inclusion bodies and amyloid. *Folding Des. 3*, R9–R23.
12. Dobson, C. M. (2001) The structural basis of protein folding and its links with human disease. *Philos. Trans. R. Soc. London, Ser. B 356*, 133–145.
13. Zerovnik, E. (2002) Amyloid-fibril formation. Proposed mechanisms and relevance to conformational disease. *Eur. J. Biochem. 269*, 3362–3371.
14. Harper, J. D., Wong, S. S., Lieber, C. M., and Lansbury, P. T., Jr. (1999) Assembly of A$\beta$ amyloid protofibrils: An in vitro model for a possible early event in Alzheimer's disease. *Biochemistry 38*, 8972–8980.
15. Uversky, V. N., Lee, H. J., Li, J., Fink, A. L., and Lee, S. J. (2001) Stabilization of partially folded conformation during $\alpha$-synuclein oligomerization in both purified and cytosolic preparations. *J. Biol. Chem. 276*, 43495–43498.
16. Uversky, V. N., Li, J., and Fink, A. L. (2001) Evidence for a partially folded intermediate in $\alpha$-synuclein fibril formation. *J. Biol. Chem. 276*, 10737–10744.
17. Gallo, G., Picken, M., Buxbaum, J., and Frangione, B. (1989) The spectrum of monoclonal immunoglobulin deposition disease associated with immunocytic dyscrasias. *Semin. Hematol. 26*, 234–245.
18. Buxbaum, J. (1992) Mechanisms of disease: Monoclonal immunoglobulin deposition. Amyloidosis, light chain deposition disease, and light and heavy chain deposition disease. *Hematol. Oncol. Clin. North Am. 6*, 323–346.
19. Solomon, A., Weiss, D. T., and Pepys, M. B. (1992) Induction in mice of human light-chain-associated amyloidosis. *Am. J. Pathol. 140*, 629–637.
20. Solomon, A. (1986) Clinical implications of monoclonal light chains. *Semin. Oncol. 13*, 341–349.
21. Solomon, A. (1985) Light chains of human immunoglobulins. *Methods Enzymol. 116*, 101–121.
22. Kaplan, B., Vidal, R., Kumar, A., Ghiso, J., Frangione, B., and Gallo, G. (1997) Amino-terminal identity of co-existent amyloid and non-amyloid immunoglobulin $\kappa$ light chain deposits. A human disease to study alterations of protein conformation. *Clin. Exp. Immunol. 110*, 472–478.
23. Sanders, P. W., and Booker, B. B. (1992) Pathobiology of cast nephropathy from human Bence Jones proteins. *J. Clin. Invest. 89*, 630–639.
24. Raffen, R., Dieckman, L. J., Szpunar, M., Wunschl, C., Pokkuluri, P. R., Dave, P., Wilkins Stevens, P., Cai, X., Schiffer, M., and Stevens, F. J. (1999) Physicochemical consequences of amino acid variations that contribute to fibril formation by immunoglobulin light chains. *Protein Sci. 8*, 509–517.
25. Pokkuluri, P. R., Raffen, R., Dieckman, L., Boogaard, C., Stevens, F. J., and Schiffer, M. (2002) Increasing protein stability by polar surface residues: Domain-wide consequences of interactions within a loop. *Biophys. J. 82*, 391–398.
26. Kabat, E. A., Wu, T. T., Perry, H. M., Gottesman, K. S., and Foeller, C. (1991) *Sequences of Proteins of Immunological Interest*, 5th ed., NIH Publication 91-3242, U.S. Department of Health and Human Services, U.S. Government Printing Office, Washington, DC.
27. Huang, D. B., Chang, C. H., Ainsworth, C., Johnson, G., Solomon, A., Stevens, F. J., and Schiffer, M. (1997) Variable domain structure of $\kappa$IV human light chain Len: High homology to the murine light chain McPC603. *Mol. Immunol. 34*, 1291–1301.
28. Stevens, P. W., Raffen, R., Hanson, D. K., Deng, Y. L., Berrios-Hammond, M., Westholm, F. A., Murphy, C., Eulitz, M., Wetzel, R., Solomon, A., et al. (1995) Recombinant immunoglobulin variable domains generated from synthetic genes provide a system for in vitro characterization of light-chain amyloid proteins. *Protein Sci. 4*, 421–432.
29. Souillac, P. O., Uversky, V. N., Millett, I. S., Khurana, R., Doniach, S., and Fink, A. L. (2002) Effect of association state and conformational stability on the kinetics of immunoglobulin light chain amyloid fibril formation at physiological pH. *J. Biol. Chem. 277*, 12657–12665.
30. Souillac, P. O., Uversky, V. N., Millett, I. S., Khurana, R., Doniach, S., and Fink, A. L. (2002) Elucidation of the molecular mechanism during the early events in immunoglobulin light chain amyloid fibrillation. Evidence for an off-pathway oligomer at acidic pH. *J. Biol. Chem. 277*, 12666–12679.
31. Souillac, P. O., Uversky, V. N., and Fink, A. L. (2003) Structural transformations of oligomeric intermediates in the fibrillation of the immunoglobulin light chain LEN. *Biochemistry 42*, 8094–8104.
32. Khurana, R., Gillespie, J. R., Talapatra, A., Minert, L. J., Ionescu-Zanetti, C., Millett, I., and Fink, A. L. (2001) Partially folded intermediates as critical precursors of light chain amyloid fibrils and amorphous aggregates. *Biochemistry 40*, 3525–3535.
33. Stadtman, E. R., and Levine, R. L. (2000) Protein oxidation. *Ann. N.Y. Acad. Sci. 899*, 191–208.
34. Stadtman, E. R. (2001) Protein oxidation in aging and age-related diseases. *Ann. N.Y. Acad. Sci. 928*, 22–38.
35. Vogt, W. (1995) Oxidation of methionyl residues in proteins: Tools, targets, and reversal. *Free Radical Biol. Med. 18*, 93–105.
36. Moskovitz, J., Bar-Noy, S., Williams, W. M., Requena, J., Berlett, B. S., and Stadtman, E. R. (2001) Methionine sulfoxide reductase (MsrA) is a regulator of antioxidant defense and lifespan in mammals. *Proc. Natl. Acad. Sci. U.S.A. 98*, 12920–12925.
37. Levine, R. L., Moskovitz, J., and Stadtman, E. R. (2000) Oxidation of methionine in proteins: Roles in antioxidant defense and cellular regulation. *IUBMB Life 50*, 301–307.
38. Peng, K., Radivojac, P., Vucetic, S., Dunker, A. K., and Obradovic, Z. (2006) Length-dependent prediction of protein intrinsic disorder. *BMC Bioinf. 7*, 208.
39. Prilusky, J., Felder, C. E., Zeev-Ben-Mordehai, T., Rydberg, E. H., Man, O., Beckmann, J. S., Silman, I., and Sussman, J. L. (2005) FoldIndex: A simple tool to predict whether a given protein sequence is intrinsically unfolded. *Bioinformatics 21*, 3435–3438.
40. Romero, P., Obradovic, Z., Li, X., Garner, E. C., Brown, C. J., and Dunker, A. K. (2001) Sequence complexity of disordered protein. *Proteins 42*, 38–48.
41. Uversky, V. N., Gillespie, J. R., and Fink, A. L. (2000) Why are "natively unfolded" proteins unstructured under physiologic conditions? *Proteins 41*, 415–427.

42. Naiki, H., Higuchi, K., Hosokawa, M., and Takeda, T. (1989) Fluorometric determination of amyloid fibrils in vitro using the fluorescent dye, thioflavin T1. *Anal. Biochem. 177*, 244–249.
43. Sreerama, N., Manning, M. C., Powers, M. E., Zhang, J. X., Goldenberg, D. P., and Woody, R. W. (1999) Tyrosine, phenylalanine, and disulfide contributions to the circular dichroism of proteins: Circular dichroism spectra of wild-type and mutant bovine pancreatic trypsin inhibitor. *Biochemistry 38*, 10814–10822.
44. Ptitsyn, O. B. (1995) Molten globule and protein folding. *Adv. Protein Chem. 47*, 83–229.
45. Semisotnov, G. V., Rodionova, N. A., Razgulyaev, O. I., Uversky, V. N., Gripas, A. F., and Gilmanshin, R. I. (1991) Study of the "molten globule" intermediate state in protein folding by a hydrophobic fluorescent probe. *Biopolymers 31*, 119–128.
46. Altschul, S. F., Madden, T. L., Schaffer, A. A., Zhang, J., Zhang, Z., Miller, W., and Lipman, D. J. (1997) Gapped BLAST and PSI-BLAST: A new generation of protein database search programs. *Nucleic Acids Res. 25*, 3389–3402.
47. Benhar, I., and Pastan, I. (1995) Identification of residues that stabilize the single-chain Fv of monoclonal antibodies B3. *J. Biol. Chem. 270*, 23373–23380.
48. Gassner, N. C., Baase, W. A., and Matthews, B. W. (1996) A test of the "jigsaw puzzle" model for protein folding by multiple methionine substitutions within the core of T4 lysozyme. *Proc. Natl. Acad. Sci. U.S.A. 93*, 12155–12158.
49. Sickmeier, M., Hamilton, J. A., LeGall, T., Vacic, V., Cortese, M. S., Tantos, A., Szabo, B., Tompa, P., Chen, J., Uversky, V. N., Obradovic, Z., and Dunker, A. K. (2007) DisProt: The Database of Disordered Proteins. *Nucleic Acids Res. 35*, D786–D793.
50. Vucetic, S., Brown, C. J., Dunker, A. K., and Obradovic, Z. (2003) Flavors of protein disorder. *Proteins 52*, 573–584.
51. Uversky, V. N. (2008) Amyloidogenesis of natively unfolded proteins. *Curr. Alzheimer's Res. 5*, 260–287.
52. Sunde, M., and Blake, C. (1997) The structure of amyloid fibrils by electron microscopy and X-ray diffraction. *Adv. Protein Chem. 50*, 123–159.
53. Walsh, D. M., Lomakin, A., Benedek, G. B., Condron, M. M., and Teplow, D. B. (1997) Amyloid $\beta$-protein fibrillogenesis. Detection of a protofibrillar intermediate. *J. Biol. Chem. 272*, 22364–22372.
54. Kisilevsky, R. (2000) Review: Amyloidogenesis-unquestioned answers and unanswered questions. *J. Struct. Biol. 130*, 99–108.
55. Gallo, G., Goni, F., Boctor, F., Vidal, R., Kumar, A., Stevens, F. J., Frangione, B., and Ghiso, J. (1996) Light chain cardiomyopathy. Structural analysis of the light chain tissue deposits. *Am. J. Pathol. 148*, 1397–1406.
56. Stokes, M. B., Jagirdar, J., Burchstin, O., Kornacki, S., Kumar, A., and Gallo, G. (1997) Nodular pulmonary immunoglobulin light chain deposits with coexistent amyloid and nonamyloid features in an HIV-infected patient. *Mod. Pathol. 10*, 1059–1065.
57. Qin, Z., Hu, D., Zhu, M., and Fink, A. L. (2007) Structural characterization of the partially folded intermediates of an immunoglobulin light chain leading to amyloid fibrillation and amorphous aggregation. *Biochemistry 46*, 3521–3531.
58. Humphrey, W., Dalke, A., and Schulten, K. (1996) VMD: visual molecular dynamics. *J. Mol. Graphics 14*, 33–38, 27−38.

BI800806D